Applied Catalysis B: Environmental 300 (2022) 120753

Contents lists available at ScienceDirect

Applied Catalysis B: Environmental

journal homepage: www.elsevier.com/locate/apcatb

Methanol electroreforming coupled to green hydrogen production over bifunctional NiIr-based metal-organic framework nanosheet arrays

You Xu, Mengying Liu, Mingzhen Wang, Tianlun Ren, Kaili Ren, Ziqiang Wang, Xiaonian Li, Liang Wang, Hongjing Wang *

State Key Laboratory Breeding Base of Green-Chemical Synthesis Technology, College of Chemical Engineering, Zhejiang University of Technology, Hangzhou 310014, PR China

ARTICLE INFO

Keywords:
Hydrogen production
Methanol electroreforming
Bifunctional electrocatalysts
Metal-organic framework
Nanosheets

ABSTRACT

The conventional water electrolysis system is seriously restricted by the sluggish kinetics of anodic oxygen evolution reaction. Electroreforming of organic substances coupling with electrochemical hydrogen evolution is an innovative strategy to achieve energy-saving co-generation of value-added chemicals and hydrogen. Herein, NiIr-based metal-organic framework (MOF) nanosheet arrays are in situ grown on Ni foam (NiIr-MOF/NF) and employed as a bifunctional self-supported electrocatalyst to oxidize small organic molecules of methanol to the value-added chemical formate while efficiently facilitating hydrogen production. The constructed co-electrolytic system based on HER-methanol oxidation reaction (MOR) bifunctional NiIr-MOF/NF electrocatalyst possesses ultra-high energy conversion efficiency for electrochemically assisted overall water splitting, with a low cell voltage of only 1.39 V to achieve the current density of 10 mA cm^{-2}. Especially, the Faradaic efficiencies of the cathode and anode could both reach nearly 100% for H_2 and formate generated in 1 M KOH containing 4 M methanol.

1. Introduction

With the rapid increase in global environmental problems caused by the consumption of fossil energy, the search for sustainable green energy has become an urgent need. Hydrogen (H_2) is attracting a lot of attention as a promising clean, renewable energy [1–6]. Currently, H_2 is mainly derived from steam reforming of fossil fuels (methane or coal) in industrial production as well as electrocatalytic hydrocracking. The use of fossil fuels is known to be highly polluting and non-recyclable. Therefore, the development of sustainable H_2 production via water electrolysis is essential to meet future global energy needs [7–13]. Unfortunately, conventional water electrolysis system is very wasteful of electrical energy and the efficiency is severely hampered by the slow kinetics of the anodic oxygen evolution reaction (OER) [14,15]. Although a number of advanced OER electrocatalysts have been reported to improve the overall energy conversion efficiency, that still do not exhibit considerable results [16–22]. Therefore, a further promising and meaningful strategy would be to replace OER by using thermodynamically more favourable oxidation reactions, especially those could generate value-added products [23,24]. Undoubtedly, the choice of a widely available, highly active, structurally simple, low-priced and easily oxidizable small molecule is crucial. To date, the assisted electrochemical hydrolysis of organic molecules such as urea [25,26], hydrazine [27,28], alcohols [29–33], amines [34–36], furanal and 5-hydroxymethylfuranal [37,38] has been reported in the literature. Among them, methanol, which has the simplest structure, becomes an ideal substrate molecule to participate in anode oxidation, and the highly selective conversion of methanol to value-added formate rather than CO_2 is of great importance. Therefore, it is highly desirable to combine methanol oxidation reaction (MOR) with hydrogen evolution reaction (HER) to construct hybrid water electrolysis systems for the simultaneous production of high purity hydrogen and high value-added chemicals.

Most previously developed HER and MOR catalysts are mainly based on Pt-based materials [39]. However, the large-scale commercial application of Pt is undoubtedly limited due to its low abundance and high cost. Recent advances have demonstrated a series of earth-rich transition metal-based catalysts and their derivatives for HER or MOR, with special attention is paid to nickel (Ni)-based nanomaterials [40–44]. As for MOR, the selection of Ni-based materials could avoids

* Corresponding author.
E-mail address: hjw@zjut.edu.cn (H. Wang).

https://doi.org/10.1016/j.apcatb.2021.120753
Received 28 July 2021; Received in revised form 8 September 2021; Accepted 23 September 2021
Available online 25 September 2021

the material shortage, poor stability and susceptibility to poisoning of precious metal catalysts and the over-oxidation that results in conventional methanol oxidation processes (producing worthless CO_2) [45]. Among various materials, graphene and other graphene analogues with two-dimensional morphology are ideal material platforms to construct catalysts with high performance [46,47]. In this regard, metal-organic frameworks (MOFs) with two-dimensional morphology have attracted increasing attentions due to their integrated merits of MOF structure (e.g., high porosity and abundant catalytic molecular units) and ultrathin 2D morphology (e.g., highly accessible active sites) [48]. When constructing Ni-based MOF catalytic materials, structural design of metal nodes is a powerful strategy to elevate the catalytic performances, since the introduced second metal center could modulate the electronic structure and coordination environment to enhance the intrinsic activity of the catalyst. Especially, some recent studies have focused on Ni-based binary MOF catalytic structures with minimal noble metal contents (e.g., Ru, Ir) for achieving a high electrocatalytic activity [49–51]. In addition, in order to achieve a faster mass and charge transfer rate, directly growing well-designed nanostructured catalysts on suitable conductive substrates is useful to form self-supported electrodes, since it can reduce the complex pre-treatment of catalytic materials and avoid the use of binders or adhesive [52]. Despite the achieved advances in HER and MOR electrocatalysis, there are still a very limited number of reports on the selective oxidation of organic molecules to coproduce value-added chemicals and high-purity hydrogen by employing 2D Ni-based MOF as self-supported HER-MOR bifunctional electrodes [53–57].

Herein, Ir-doping Ni-based MOF (Ir-doped $Ni_2(BDC)_2TED$, BDC = 1,4-benzenedicarboxylic acid, TED = triethylenediamine) nanosheet arrays on Ni foam (NiIr-MOF/NF) were developed and employed as bifunctional electrocatalysts for coupling HER and MOR to simultaneous production of hydrogen and valuable formate. For the constructed NiIr-MOF/NF ||NiIr-MOF/NF two-electrode co-electrocatalytic system, a cell voltage of only 1.39 V is needed to realize a geometrical catalytic current density of 10 mA cm^{-2} in 1 M KOH containing 4 M methanol, which decreased by 170 mV after replacing the OER with MOR. Notably, the NiIr-MOF/NF was demonstrated to perform high Faradaic efficiencies (FE) (close to 100%) for both hydrogen and formate generation. This work experimentally proved the excellent methanol oxidation properties of MOF-based materials, providing new insights to design hybrid water electrolysis systems for simultaneously electrocatalytic production of value-added fine chemicals and hydrogen by replacing the conventionally energy-intensive chemical technologies.

2. Experimental section

2.1. Reagents and chemicals

Nickel (II) nitrate hexahydrate (Ni $(NO_3)_2.6H_2O$), N, N-dimethylformamide (DMF/$HCON(CH_3)_2$) were acquired from Adamas Reagent Co., Ltd. (Shanghai, China). Iridium chloride hydrate ($IrCl_3{\cdot}xH_2O$), 1,4-benzenedicarboxylic acid (BDC/$C_8H_6O_4$), triethylenediamine (TED/$C_6H_{12}N_2$), ruthenium oxide (RuO_2), and commercial Pt/C (20 wt%) were provided from Aladdin Industrial Corporation (Shanghai, China).

2.2. Synthesis of the NiIr-MOF/NF

The NiIr-MOF/NF was synthesized according to our previous study with minor modifications [49]. Typically, a piece of Ni foam (2 cm × 4 cm) was pretreated with dilute HCl (3 M) for about 15 min. Then, Ni $(NO_3)_2.6H_2O$ (0.3 g), TED (0.033 g) and BDC (0.105 g) were dispersed in 30 mL DMF under sonication to form a transparent green solution. Next, 3 mL of $IrCl_3$ aqueous solution (20 mM) was added into the mixture with intense stirring for 15 min. After that, the mixed solution and a piece of the pretreated Ni foam were heated at 130 °C for 24 h in a 50 mL Teflon-lined autoclave. Finally, when it naturally cooled to ambient temperature, the NiIr-MOF/NF could be obtained after washing with absolute ethanol several times and drying at 50 °C overnight. For follow-up comparison, replace 3 mL of $IrCl_3$ (20 mM) with 3 mL of deionized water to acquire the Ni-MOF/ NF counterpart.

2.3. Characterization

Scanning electron microscopy (SEM) and energy dispersive x-ray (EDX) measurements were tested on a Gemini SEM 500. Transmission electron microscopy (TEM) and high-angle annular dark field-scanning transmission electron microscopy (HAADF-STEM) were carried out on a FEI Talos F200X. X-ray powder diffraction (XRD) was performed using a X′Pert PRO MPD. X-ray Photoelectron Spectroscopy (XPS) was obtained by an ESCALAB 250XL spectrometer. Nuclear magnetic resonance (NMR) spectrometer was carried on a Bruker Avance NEO 600. Inductively coupled plasma optical emission spectrometry (ICP-OES) was analyzed using a Aglient 7800.

2.4. Electrochemical investigation

The MOR, HER, and OER electrochemical activities of the catalysts were evaluated by a conventional three-electrode system on a CHI 660E electrochemical workstation (counter electrode: graphite rod, reference electrode: Ag/AgCl electrode). The as-made NiIr-MOF/NF was cut into 1 cm × 1 cm and directly used as the working electrode. The current densities of the HER and MOR were normalized to the geometric area of Ni foam substrate and all of the tested potentials were assessed as the reversible hydrogen electrode (RHE) scale according to Nernst equation ($E_{vs.RHE} = E^0_{Ag/AgCl} + E_{vs.Ag/AgCl} + 0.059$*pH). Linear sweep voltammetry (LSV) curves were tested in 1.0 M KOH with and without 4 M methanol (5 mV s^{-1}). As for the Pt/C/NF and RuO_2/NF electrodes, the amount of Pt/C (20 wt%) and RuO_2 loaded on the electrode (Ni foam substrate, 1 cm × 1 cm) was 1 mg (see Fig. S1 for TEM images of Pt/C and RuO_2). Electrochemical impedance spectroscopy (EIS) was carried out at 1.4 V for MOR and −0.05 V for HER, respectively, which was recorded from 100 kHz to 0.1 Hz with the amplitude of 5 mV. All the electrochemical measurements were carried out at around 25 °C.

As for HER-MOR co-electrolytic system, the NiIr-MOF/NF was used as both the anode and cathode for constructing two-electrode setup. The generated H_2 and formate in two-electrode system were quantified by water drainage method and ^1H NMR spectroscopy, respectively. Maleic acid was used as an internal standard in NMR analysis. The corresponding FE is calculated by the following equation: $FE = (N \times Z \times F/Q) \times 100\%$, where N is the mole of product (H_2 or formate) produced, Q is the passed charge, F is the Faraday constant (96,485 C mol^{-1}), and Z is the number of electrons transferred for a mole of H_2 ($Z = 2$) and formate ($Z = 4$) formation [58].

3. Results and discussion

3.1. Characterization of NiIr-MOF/NF

The NiIr-MOF/NF composite was obtained according to the previously developed solvothermal method with some minor modifications [49], as schematically illustrated in Fig. 1a. For comparison in later electrochemical studies, the Ni-MOF/NF counterpart was also prepared (Fig. S2). The morphologies of the as-obtained NiIr-MOF/NF sample were examined by SEM, as shown in Fig. 1b and c. Highly dense nanosheets, 2–4 μm in lateral size and approximately 10 nm in thickness, were grown vertically on the surface of Ni foam substrate. In more detail, the ultrathin nanosheet morphology of MOF structure is further evidenced and characterized by TEM (Fig. 1d). The composition analysis of these NiIr-MOF nanosheets was performed by using EDX spectroscopy, revealing the existence of Ni, Ir, C, N and O elements (Fig. S3). Quantitative analysis by ICP-OES reveal that the Ir/Ni molar ratio in NiIr-MOF nanosheets is 2.35/100, which is close to the EDX result

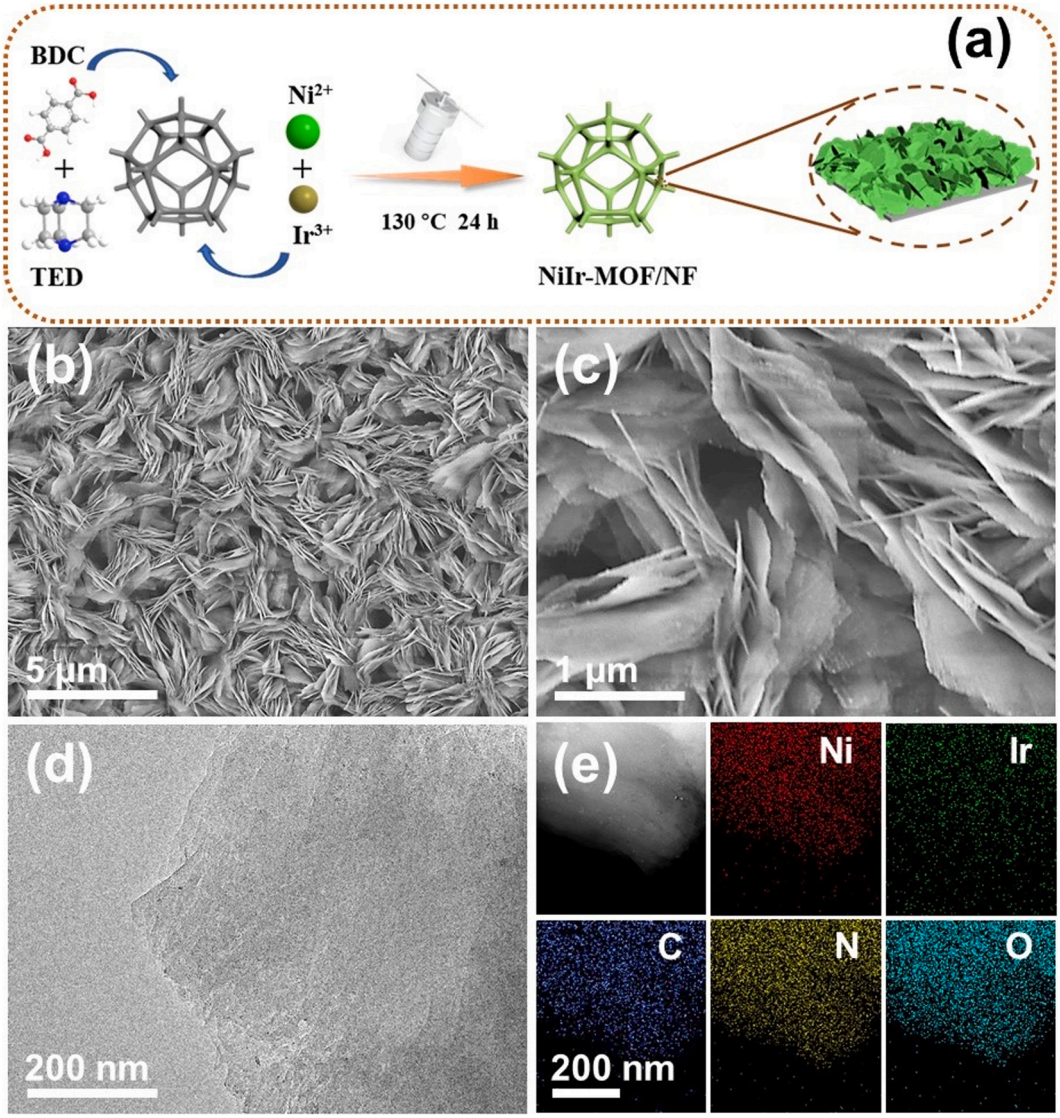

Fig. 1. (a) Schematic illustration of the synthetic process of the NiIr-MOF/NF. (b,c) SEM images of the NiIr-MOF/NF. (d) TEM image and (e) HAADF-STEM and corresponding elemental mappings of NiIr-MOF nanosheets.

(Ir/Ni = 2.2/100). In addition, HAADF-STEM and element mapping analysis in Fig. 1e show that the Ni, Ir, C, N and O elements are uniformly distributed in the whole MOF nanosheets.

XRD was conducted to investigate the crystal structure of the MOF catalyst. As displayed in Fig. 2a, the Ni-MOF sample showed typical XRD pattern characteristics of $M_2(BDC)_2TED$ MOF structure [59]. It can be seen that the crystal structure of NiIr-MOF is similar to that of Ni-MOF, suggesting that low content of Ir doping do not change the crystal structure of Ni-MOF, as also demonstrated in previous studies [49]. The surface chemical composition and elemental valence state of the NiIr-MOF were acquired through XPS. Being consistent with both the EDX and elemental mapping results, the XPS survey spectrum of the NiIr-MOF nanosheets suggests the presence of C, N, O, Ni and Ir elements (Fig. S4). In the high-resolution Ni 2p spectrum (Fig. 2b), two obvious peaks at 855.9 and 873.65 eV were identified as Ni^{2+} $2p_{3/2}$ and Ni^{2+} $2p_{1/2}$, and the peaks at 861.3 and 879.7 eV can be attributed to two satellite peaks [50,60]. In comparison to Ni-MOF (Ni^{2+} $2p_{3/2}$ at 856.1 eV and Ni^{2+} $2p_{1/2}$ at 873.8 eV), the binding energies of NiIr-MOF show a slightly negative shift (0.2 eV) (Fig. S5), suggesting that the incorporation of Ir cations into the MOF structure caused a change in the electronic structure and coordination environment of the Ni cations [50,51]. As depicted in Fig. 2c for the Ir 4f spectrum, the major peaks can be deconvoluted at 61.3 and 64.4 eV, which are related to $4f_{7/2}$ and $4f_{5/2}$ of $Ir^{\delta+}$ species in the MOF structure [61]. Moreover, The C 1s, N 1s and O 1s XPS spectra were presented in Fig. 2d-f. In the C 1s spectrum, the peaks at 284.6, and 288.2 eV can be assigned to C═C and O–C═O in the NiIr-MOF structure (Fig. 2d). And the peak located at 399.3 eV can be observed to N 1s (Fig. 2e). As for the O 1s spectrum (Fig. 2f), three contributions appearing at 532.2, 531.4, and 530.8 eV belong to Ni (Ir)–O, O–C═O, and absorbed water, respectively [54,62].

3.2. Electrocatalytic performances for MOR

Electrochemical upgrading of methanol is attractive given its potential to be converted into value-added products such as formate. The responsiveness of as-fabricated NiIr-MOF/NF to anodic oxidation of methanol were first investigated and relevant electrochemical tests were performed under a typical three-electrode system. Corresponding data are shown in Fig. 3. Firstly, the self-supported NiIr-MOF/NF was tested in the presence and absence of methanol at 1.0 M KOH to obtain LSV curves, and Fig. 3a shows that the electrode exhibited a high MOR responsiveness after the introduction of methanol. It can be obviously observed that, as the methanol concentration increases (e.g., from 0 M to 4 M), the required applied potential at the same current density

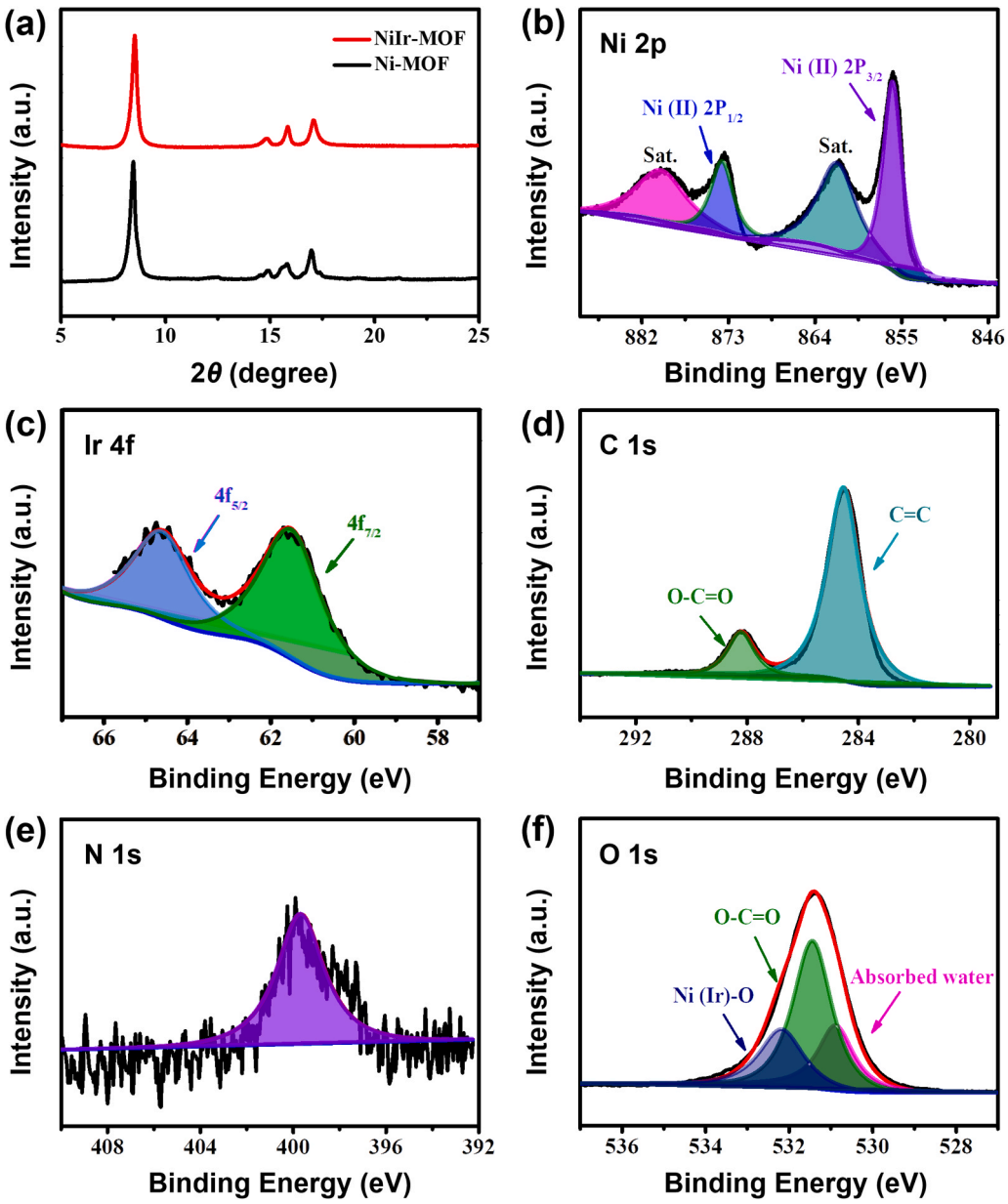

Fig. 2. (a) XRD patterns of Ni-MOF nanosheets and NiIr-MOF nanosheets. XPS spectra of (b) Ni 2p, (c) Ir 4f, (d) C 1s, (e) N 1s, and (f) O 1s for NiIr-MOF nanosheets.

gradually decreases. However, when the methanol increases infinitely (e.g., form 4–8 M), the MOR activity shows the opposite trend. This may be due to the adsorption of pre-existing oxidation products on the electrode surface preventing further oxidation reactions [58]. Considering the utilization efficiency of methanol, we choose 4 M as the finally optimized concentration. Apparently, the addition of 4 M methanol in electrolyte reduces the overpotential by 170 mV at 100 mA cm^{-2}, compared with that in 1.0 M KOH solution without methanol (i.e., OER curve). In the OER polarization curve, the peak at about 1.4 V (vs.RHE) can be attributed to Ni^{2+}/Ni^{3+}. As demonstrated in literature, the Ni^{2+}/Ni^{3+} species function as the active species for anode oxidation of organic molecules [63].

In comparison with the high oxidation potentials of MOR on Ni-MOF/NF, RuO_2/NF and blank NF, the NiIr-MOF/NF exhibit higher performance (Fig. 3b). For instance, to yield the 10 and 100 mA cm^{-2}, the required applied potential on the NiIr-MOF/NF is 1.33 and 1.41 V (vs. RHE), respectively, which are lower than Ni-MOF/NF (1.39 V @ 10 mA cm^{-2}, 1.44 V @ 100 mA cm^{-2}), RuO_2/NF (1.36 V @ 10 mA cm^{-2}, 1.46 V @ 100 mA cm^{-2}) and blank NF (1.40 V @ 10 mA cm^{-2}, 1.47 V @ 100 mA cm^{-2}). For investigating the MOR kinetics mechanism on the electrocatalysts, Tafel plots were obtained by fitting the corresponding LSV curves. From Fig. 3c, the Tafel slop of NiIr-MOF/NF for MOR is calculated to be 17.7 mV dec^{-1}, which is substantially lower than Ni-MOF/NF (52.5 mV dec^{-1}), RuO_2/NF (90.5 mV dec^{-1}) and NF (96.9 mV dec^{-1}), implying a faster electrochemical kinetic process on the NiIr-MOF/NF. Meanwhile, the Tafel slope of MOR is smaller than the OER (114.2 mV dec^{-1}) when methanol is not introduced, which is a sufficient indication that the presence of methanol leads to a vast improvement of the catalytic kinetics at the NiIr-MOF/NF anode. (Fig. S6) The EIS measurements present that the charge transfer resistance of NiIr-MOF/NF is smaller than that of Ni-MOF/NF, RuO_2/NF and NF (Fig. S7a). Based on the above Tafel slope and EIS results, it can be well proven that NiIr-MOF/NF has faster reaction kinetics and higher electron transfer ability in the MOR operating system. Furthermore, long-term cyclic voltammetry (CV) cycling and chronoamperometry (i-t) measurements were further studied to assess the stability and durability of the NiIr-MOF/NF electrode toward MOR. The LSV curves for NiIr-MOF/NF electrode did not show obvious float

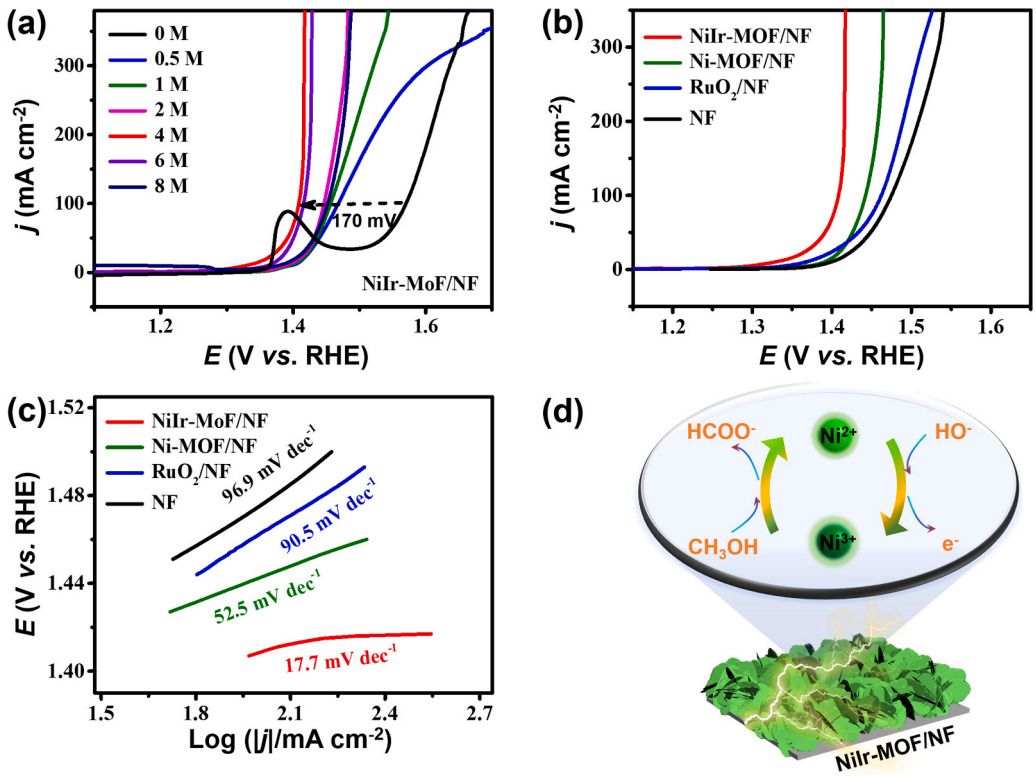

Fig. 3. (a) LSV curves (with iR correction) for the NiIr-MOF/NF electrodes with different concentrations of methanol in 1 M KOH. (b) LSV curves (with iR correction) for various electrodes collected in 1 M KOH containing 4 M methanol. (c) Tafel plots on different electrodes. (d) The proposed redox cycle between Ni^{2+} and Ni^{3+} for the electrocatalytic conversion from methanol to formate.

before and after 2000 continuous CV cycles (Fig. S8a) and the i-t operation over 12 h at a 1.4 V (vs. RHE) applied potential (Fig. S8b), demonstrated the robust catalytic durability for MOR.

It is noted that the NiIr-MOF/NF electrode has ultra-low overpotential, fast kinetics, and high electrocatalytic stability for methanol oxidation, realizing the possibility of upgrading multiple organic molecules of simple structure into value-added products, substituting for OER, and providing realism for reducing energy consumption. In the NiIr-MOF structure, Ni sites are considered the catalytically active sites and the in situ generated Ni^{2+}/Ni^{3+} species under anodic potentials function as the active species for oxidation of methanol molecules. Above-mentioned XPS results have revealed the modified electronic structure and coordination environment of Ni sites due to Ir incorporation, which could lead to enhance the electrocatalytic performance [49,64]. As shown in Fig. S9, both the onset and peak potentials of Ni^{2+}/Ni^{3+} for NiIr-MOF/NF are lower than those of Ni-MOF/NF, suggesting the incorporation of Ir cations into the Ni-MOF structure facilitates the generation of Ni^{2+}/Ni^{3+} species under anodic potentials. The electrocatalytic methanol oxidation process over the NiIr-MOF/NF is schematically illustrated Fig. 3d. Under appropriate anodic potentials and alkaline conditions, Ni^{2+} in coordination center combines with hydroxide to be oxidized to high-valent Ni^{3+} [45, 65–67]. Subsequently, the nucleophilic species methanol can easily adsorb the activated nickel and be oxidized to value-added formic acid. The Ni^{3+} is reduced to Ni^{2+} to restart the MOR cycle, simultaneously.

3.3. Electrocatalytic performances for HER

Unlike most studies on MOF-derived electrocatalyst materials, the as-prepared NiIr-MOF/NF was directly acted as a working electrode for electrochemical HER. Fig. 4a displays the HER polarization curves of various electrocatalysts, suggesting the higher HER performance on the NiIr-MOF/NF. At a cathodic current density of 10 mA cm^{-2}, the NiIr-MOF/NF needs the lowest overpotential of only 17 mV (η_{10} = 17 mV), compared with Ni-MOF/NF (η_{10} = 123 mV), Pt/C/NF (η_{10} = 24 mV) and NF (η_{10} = 183 mV) (Fig. 4b). Electrocatalytic HER kinetics is assessed by Tafel slops. As shown in Fig. 4c, the Tafel slop of NiIr-MOF/NF (63.6 mV dec^{-1}) is much lower than Ni-MOF/NF (92.4 mV dec^{-1}), NF (175.6 mV dec^{-1}), and slightly higher than the Pt/C/NF (51.4 mV dec^{-1}), indicating the NiIr-MOF/NF has faster catalytic reaction kinetics. Considering the combination of anodic methanol oxidation with cathodic HER, the electrode must have a stable catalytic activity towards HER in the presence of methanol. As expected, the adding of methanol nearly has no impact on the cathodic HER activity (Fig. 4d). Moreover, the EIS analysis (Fig. S7b) of NiIr-MOF/NF also demonstrated low electron transfer resistance and a fast electron transfer rate at the cathode in 1 M KOH solution. Double layer capacitance (C_{dl}) is evaluated to measure the electrochemically active surface area (ECSA). As shown in Fig. S10, the capacitance for NiIr-MOF/NF was calculated to be 5.5 mF cm^{-2} based on the CV results, higher than that of Ni-MOF/NF (1.7 mF cm^{-2}). According to the equation: ECSA = $S_{geo} \times C_{dl}/C_s$. ("$C_s$" represents specific C_{dl}, which is 0.040 mF cm^{-2} under alkaline conditions and the "S_{geo}" is the geometric surface area of the working electrode (1 cm^2)). The ECSA of NiIr-MOF/NF was calculated to be 137.5 cm^2, which is larger than that of Ni-MOF/NF (42.5 cm^2) [68,69]. This is also an important factor leading to its high electrocatalytic activity. In addition, in order to clearly show the superiority of HER, 7000 CV cycles tests and 12 h chronopotentiometry (V-t) stability tests were carried out (Fig. 4e and Fig. 4f). By comparing the polarization curves (close to coincidence) before (η_{10} = 17 mV) and after (η_{10} = 20 mV) the CV test, as well as the overpotential did not significantly decrease from the V-t curve at 10 mA cm^{-2} for 12 h, it can be well illustrated that NiIr-MOF/NF as cathode material has excellent durability and electrochemical stability for HER.

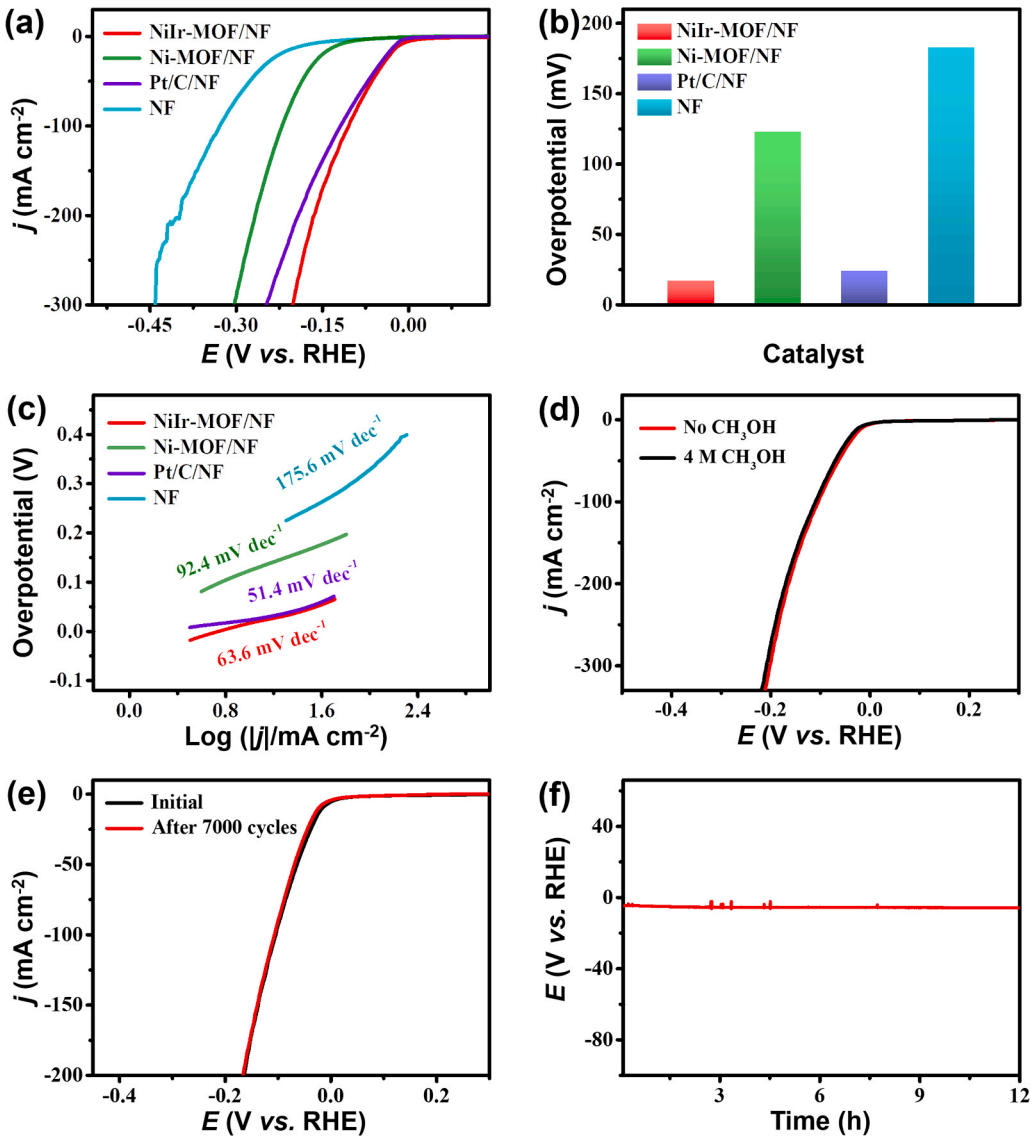

Fig. 4. (a) HER polarization curves for various catalysts in 1.0 M KOH solution and (b) comparison of the required overpotential at a current density of 10 mA cm^{-2} for various catalysts. (c) Tafel plots on various electrodes. (d) HER polarization curves for NiIr-MOF/NF in 1 M KOH solution with and without 4 M methanol addition. (e) HER polarization curves for NiIr-MOF/NF before and after 7000 CV tests. (d) The V-t curve of NiIr-MOF/NF with constant cathodic current density of 10 mA cm^{-2} for 12 h. All of the polarization curves were iR corrected.

3.4. Electrochemical performances of the two-electrode system by integrating MOR with HER

Based on the above, NiIr-MOF/NF as a working electrode has remarkable electrochemical performance for both the anodic MOR and the cathodic HER, demonstrating its superior HER-MOR bifunctional electrolytic properties. We then constructed the HER-MOR co-electrolytic system in 1 M KOH solution containing 4 M methanol by employing the NiIr-MOF/NF as both anode and cathode (NiIr-MOF/NF || NiIr-MOF/NF) and the corresponding catalytic device diagram is shown in Fig. 5a. The overall water splitting performance of NiIr-MOF/NF ||NiIr-MOF/NF was also tested in 1 M KOH solution without methanol for comparison. As shown in Fig. 5b, in the case of methanol introduced, a cell voltage of 1.39 V is needed to achieve the current density of 10 mA cm^{-2} in 1 M KOH containing 4 M methanol, while that in the absence of methanol is 1.56 V (that is the conventional overall water splitting). Impressively, the performance of NiIr-MOF/NF||NiIr-MOF/NF system is also superior to that of Ni-MOF/NF ||Ni-MOF/NF system under the same conditions (1.52 V @ 10 mA cm^{-2}) (Fig. S11), and surpasses many recently reported alcohol selective oxidation-assisted hydrogen production systems (Table S1), demonstrating that the incorporation of Ir into Ni-MOF structure and the introduction of methanol can significantly reduce the overpotential required for electrolysis. For NiIr-MOF/NF ||NiIr-MOF/NF, the replacement of OER with MOR shows great potential to achieve energy-efficient hydrogen production. The amount of H_2 generated experimentally at a cell voltage of 1.8 V is close to the theoretical calculation value (Fig. 5c), and the hydrogen evolution FE is as high as 98.5%. In order to further clarify the electrolytic products of the anode, we further examined the products at different intervals by NMR spectrometer (Fig. 5d) and found that the FE of formate reached about 95% (Fig. 5e) and no other organic molecules was found, at the same time, there were no bubbles emerging from the surface of the anode electrode. In addition, considering the effect of different voltages on the anode product, FEs for formate of 1.4 V, 1.6 V, 1.8 V, 2.0 V and even 2.2 V were calculated (Fig. S12). Despite increased competition from OER at higher voltages, the achieved FEs for formate produced at these cell voltages still exceed 92%. It is explained in the literature that the impressive FE may be attributed to the incomplete oxidation of methanol by the catalyst [67,70]. Chronopotentiometry (V-t) measurement was performed to evaluate the long-term stability of this two-electrode system. When the measured current density set at constant 10 mA cm^{-2}, the V-t curve shows that the required cell voltage does not change significantly (Fig. 5f), suggesting the excellent catalytic stability. Moreover, the SEM, TEM and corresponding element mapping images and XPS analysis on the post-electrolysis catalysts further confirm the stability of the electrocatalysts from the morphology,

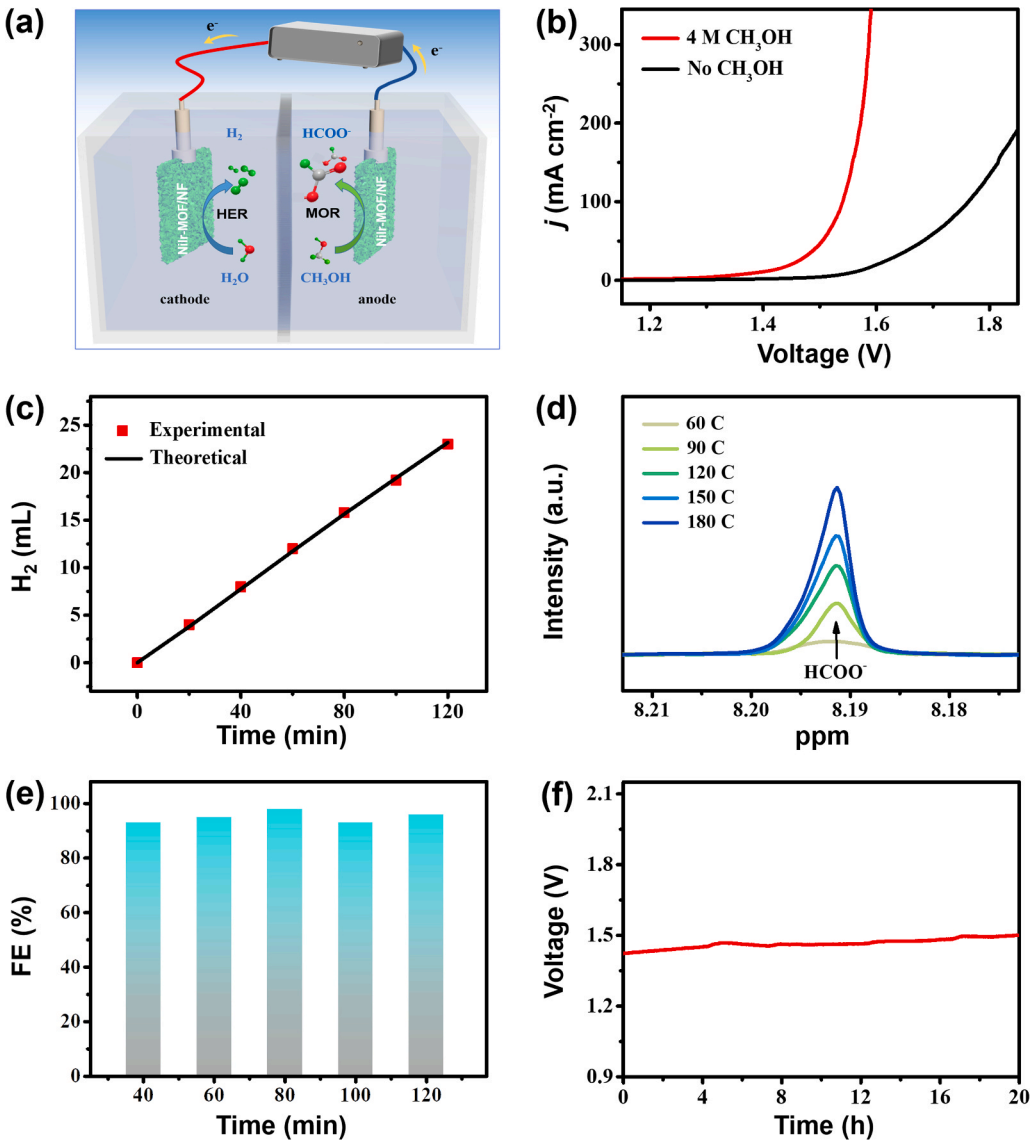

Fig. 5. Electrochemical performances of NiIr-MOF/NF||NiIr-MOF/NF: (a) Schematic illustration of concurrent electrolytic hydrogen and formate productions from methanol solution for NiIr-MOF/NF ||NiIr-MOF/NF system. (b) LSV curves in 1.0 M KOH solution with and without 4 M methanol addition for the NiIr-MOF/NF ||NiIr-MOF/NF system. (c) The measured H_2 amount and theoretical values on cathodic. (d) ^1H NMR measurements of methanol oxidation to formate on anode at 1.8 V in 1.0 M KOH solution with 4 M methanol addition. (e) The FE for formate production on anode. (f) The V-t curve of NiIr-MOF/NF ||NiIr-MOF/NF with constant current density of 10 mA cm^{-2} for 20 h. The polarization curves in (b) were iR corrected.

structure and composition (Figs. S13–S16). The above stability tests illustrate the great potential of NiIr-MOF/NF as a dual-function self--supported electrode for HER and MOR, thus achieving value-added formate in conjunction with hydrogen production.

The excellent electrocatalytic performance of NiIr-MOF/NF for HER and MOR is mainly due to the synergistically enhanced microstructural and compositional advantages. Firstly, NiIr-MOF/NF with binary MOF structure and 2D ultrathin sheet morphology can provide a large amount of catalytic active sites due to their high porosity and abundant surface area [49,50]. Secondly, incorporation of low-content of Ir cations into the Ni-MOF structure could effectively modulate the electronic structure and local coordination environment of Ni sites, which could optimize the adsorption properties of H_2O molecule, methanol molecule, and related reaction intermediates during electrochemical processes, and thus boost the electrocatalytic activity for HER and MOR [51,64,71]. Thirdly, the design of self-supported electrodes avoids the use of binders, which could lead to efficient mass and charge transfer, as well as enhanced reaction kinetics [52].

4. Conclusions

In summary, NiIr-MOF/NF nanosheet arrays are grown on Ni foam and function as a bifunctional self-supported electrode for energy-efficient H_2 production by substituting OER with MOR. The constructed NiIr-MOF/NF ||NiIr-MOF/NF two-electrode system could derive a current density of 10 mA cm^{-2} with a cell voltage of 1.39 V in methanol-water electrolyte by co-electrolysis, much lower than that of overall water splitting (1.56 V). More exciting, the NiIr-MOF/NF electrode exhibits the excellent HER and superior MOR catalytic properties, the FEs of H_2 at the cathode and formate at anode are all close to 100%. This will significantly improve the energy conversion efficiency and reduce energy consumption. This study may open up new future research trend for the use of MOF and MOF-based composites for the design of coupled co-electrolytic cells, enriching their direct application in the field of energy electrocatalysis.

CRediT authorship contribution statement

You Xu: Experimental Measurements, Data analysis, Manuscript Preparation. **Mengying Liu:** Experimental Measurements, Data analysis. **Mingzhen Wang:** Experimental Measurements. **Tianlun Ren:** Data curation. **Kaili Ren:** Data curation. **Ziqiang Wang:** Writing – review & editing. **Xiaonian Li:** Supervision. **Liang Wang:** Conceptualization, Supervision, Funding acquisition. **Hongjing Wang:** Writing – review &

editing, Supervision, Project administration.

Declaration of Competing Interest

The authors declare that they have no known competing financial interests or personal relationships that could have appeared to influence the work reported in this paper.

Acknowledgements

This work was financially supported by the National Natural Science Foundation of China (No. 21601154, 21701141, 21972126, 21978264, 21905250).

Appendix A. Supporting information

Supplementary data associated with this article can be found in the online version at doi:10.1016/j.apcatb.2021.120753.

References

[1] J. Zhu, L. Hu, P. Zhao, L.Y.S. Lee, K.Y. Wong, Recent advances in electrocatalytic hydrogen evolution using nanoparticles, Chem. Rev. 120 (2020) 851–918, https://doi.org/10.1021/acs.chemrev.9b00248.

[2] C.-T. Dinh, A. Jain, F.P.G. de Arquer, P. De Luna, J. Li, N. Wang, X. Zheng, J. Cai, B. Z. Gregory, O. Voznyy, B. Zhang, M. Liu, D. Sinton, E.J. Crumlin, E.H. Sargent, Multi-site electrocatalysts for hydrogen evolution in neutral media by destabilization of water molecules, Nat. Energy 4 (2018) 107–114, https://doi.org/10.1038/s41560-018-0296-8.

[3] I. Staffell, D. Scamman, A. Velazquez Abad, P. Balcombe, P.E. Dodds, P. Ekins, N. Shah, K.R. Ward, The role of hydrogen and fuel cells in the global energy system, Energy Environ. Sci. 12 (2019) 463–491, https://doi.org/10.1039/c8ee01157e.

[4] W. Zhong, S. Shen, M. He, D. Wang, Z. Wang, Z. Lin, W. Tu, J. Yu, The pulsed laser-induced Schottky junction via in-situ forming Cd clusters on CdS surfaces toward efficient visible light-driven photocatalytic hydrogen evolution, Appl. Catal. B: Environ. 258 (2019), 117967, https://doi.org/10.1016/j.apcatb.2019.117967.

[5] Y. Xu, K. Ren, T. Ren, M. Wang, S. Yu, Z. Wang, X. Li, L. Wang, H. Wang, Phosphorus-triggered modification of the electronic structure and surface properties of Pd4S nanowires for robust hydrogen evolution electrocatalysis, J. Mater. Chem. A 8 (2020) 19873–19878, https://doi.org/10.1039/d0ta07403a.

[6] W. Zhong, Z. Wang, N. Gao, L. Huang, Z. Lin, Y. Liu, F. Meng, J. Deng, S. Jin, Q. Zhang, L. Gu, Coupled vacancy pairs in Ni-doped CoSe for improved electrocatalytic hydrogen production through topochemical deintercalation, Angew. Chem. Int. Ed. Engl. 59 (2020) 22743–22748, https://doi.org/10.1002/anie.202011378.

[7] J. Duan, S. Chen, C. Zhao, Ultrathin metal-organic framework array for efficient electrocatalytic water splitting, Nat. Commun. 8 (2017) 15341, https://doi.org/10.1038/ncomms15341.

[8] J. Joo, T. Kim, J. Lee, S.I. Choi, K. Lee, Morphology-controlled metal sulfides and phosphides for electrochemical water splitting, Adv. Mater. 31 (2019), 1806682, https://doi.org/10.1002/adma.201806682.

[9] T. Ouyang, Y.Q. Ye, C.Y. Wu, K. Xiao, Z.Q. Liu, Heterostructures composed of N-doped carbon nanotubes encapsulating cobalt and beta-Mo2C nanoparticles as bifunctional electrodes for water splitting, Angew. Chem. Int. Ed. Engl. 58 (2019) 4923–4928, https://doi.org/10.1002/anie.201814262.

[10] B. Zhang, Y. Zheng, T. Ma, C. Yang, Y. Peng, Z. Zhou, M. Zhou, S. Li, Y. Wang, C. Cheng, Designing MOF nanoarchitectures for electrochemical water splitting, Adv. Mater. 33 (2021), 2006042, https://doi.org/10.1002/adma.202006042.

[11] Y. Zhu, Q. Lin, Y. Zhong, H.A. Tahini, Z. Shao, H. Wang, Metal oxide-based materials as an emerging family of hydrogen evolution electrocatalysts, Energy Environ. Sci. 13 (2020) 3361–3392, https://doi.org/10.1039/d0ee02485f.

[12] J. Xu, I. Amorim, Y. Li, J. Li, Z. Yu, B. Zhang, A. Araujo, N. Zhang, L. Liu, Stable overall water splitting in an asymmetric acid/alkaline electrolyzer comprising a bipolar membrane sandwiched by bifunctional cobalt-nickel phosphide nanowire electrodes, Carbon Energy 2 (2020) 646–655, https://doi.org/10.1002/cey2.56.

[13] Z.F. Huang, J. Song, Y. Du, S. Dou, L. Sun, W. Chen, K. Yuan, Z. Dai, X. Wang, Optimizing interfacial electronic coupling with metal oxide to activate inert polyaniline for superior electrocatalytic hydrogen generation, Carbon Energy 1 (2019) 77–84, https://doi.org/10.1002/cey2.3.

[14] Y. Shi, Y. Yu, Y. Liang, Y. Du, B. Zhang, In situ electrochemical conversion of an ultrathin tannin nickel iron complex film as an efficient oxygen evolution reaction electrocatalyst, Angew. Chem. Int. Ed. Engl. 58 (2019) 3769–3773, https://doi.org/10.1002/anie.201811241.

[15] A. Ali, P.K. Shen, Recent progress in graphene-based nanostructured electrocatalysts for overall water splitting, Electrochem. Energy Rev. 3 (2020) 370–394, https://doi.org/10.1007/s41918-020-00066-3.

[16] P. Li, R. Zhao, H. Chen, H. Wang, P. Wei, H. Huang, Q. Liu, T. Li, X. Shi, Y. Zhang, M. Liu, X. Sun, Recent advances in the development of water oxidation electrocatalysts at mild pH, Small 15 (2019), 1805103, https://doi.org/10.1002/smll.201805103.

[17] D. Chen, M. Qiao, Y.R. Lu, L. Hao, D. Liu, C.L. Dong, Y. Li, S. Wang, Preferential cation vacancies in perovskite hydroxide for the oxygen evolution reaction, Angew. Chem. Int. Ed. Engl. 57 (2018) 8691–8696, https://doi.org/10.1002/anie.201805520.

[18] C. Mo, J. Jian, J. Li, Z. Fang, Z. Zhao, Z. Yuan, M. Yang, Y. Zhang, L. Dai, D. Yu, Boosting water oxidation on metal-free carbon nanotubes via directional interfacial charge-transfer induced by an adsorbed polyelectrolyte, Energy Environ. Sci. 11 (2018) 3334–3341, https://doi.org/10.1039/c8ee01487f.

[19] T. Naito, T. Shinagawa, T. Nishimoto, K. Takanabe, Recent advances in understanding oxygen evolution reaction mechanisms over iridium oxide, Inorg. Chem. Front. 8 (2021) 2900–2917, https://doi.org/10.1039/d0qi01465f.

[20] J. Su, R. Ge, K. Jiang, Y. Dong, F. Hao, Z. Tian, G. Chen, L. Chen, Assembling ultrasmall copper-doped ruthenium oxide nanocrystals into hollow porous polyhedra: highly robust electrocatalysts for oxygen evolution in acidic media, Adv. Mater. 30 (2018), 1801351, https://doi.org/10.1002/adma.201801351.

[21] B. Wang, C. Tang, H.F. Wang, X. Chen, R. Cao, Q. Zhang, A nanosized CoNi hydroxide@hydroxysulfide core-shell heterostructure for enhanced oxygen evolution, Adv. Mater. 31 (2019), 1805658, https://doi.org/10.1002/adma.201805658.

[22] Y. Zhao, M. Luo, S. Chu, M. Peng, B. Liu, Q. Wu, P. Liu, F.M.F. de Groot, Y. Tan, 3D nanoporous iridium-based alloy microwires for efficient oxygen evolution in acidic media, Nano Energy 59 (2019) 146–153, https://doi.org/10.1016/j.nanoen.2019.02.020.

[23] L. Chen, J. Shi, Chemical-assisted hydrogen electrocatalytic evolution reaction (CAHER), J. Mater. Chem. A 6 (2018) 13538–13548, https://doi.org/10.1039/c8ta03741h.

[24] Y. Xu, B. Zhang, Recent advances in electrochemical hydrogen production from water assisted by alternative oxidation reactions, ChemElectroChem 6 (2019) 3214–3226, https://doi.org/10.1002/celc.201900675.

[25] Y. Xu, T.L. Ren, K.L. Ren, S.S. Yu, M.Y. Liu, Z.Q. Wang, X.N. Li, L. Wang, H. J. Wang, Metal-organic frameworks-derived Ru-dopedCo2P/N-doped carbon composite nanosheet arrays as bifunctional electrocatalystsfor hydrogen evolution and urea oxidation, Chem. Eng. J. 408 (2021), 127308, https://doi.org/10.1016/j.cej.2020.127308.

[26] Z.-Y. Yu, C.-C. Lang, M.-R. Gao, Y. Chen, Q.-Q. Fu, Y. Duan, S.-H. Yu, Ni–Mo–O nanorod-derived composite catalysts for efficient alkaline water-to-hydrogen conversion via urea electrolysis, Energy Environ. Sci. 11 (2018) 1890–1897, https://doi.org/10.1039/c8ee00521d.

[27] Z. Wang, L. Xu, F. Huang, L. Qu, J. Li, K.A. Owusu, Z. Liu, Z. Lin, B. Xiang, X. Liu, K. Zhao, X. Liao, W. Yang, Y.B. Cheng, L. Mai, Copper–Nickel Nitride nanosheets as efficient bifunctional catalysts for hydrazine-assisted electrolytic hydrogen production, Adv. Energy Mater. 9 (2019), 1900390, https://doi.org/10.1002/aenm.201900390.

[28] J.Y. Zhang, H. Wang, Y. Tian, Y. Yan, Q. Xue, T. He, H. Liu, C. Wang, Y. Chen, B. Y. Xia, Anodic hydrazine oxidation assists energy-efficient hydrogen evolution over a bifunctional cobalt perselenide nanosheet electrode, Angew. Chem. Int. Ed. Engl. 57 (2018) 7649–7653, https://doi.org/10.1002/anie.201803543.

[29] H. Huang, C. Yu, X. Han, H. Huang, Q. Wei, W. Guo, Z. Wang, J. Qiu, Ni, Co hydroxide triggers electrocatalytic production of high-purity benzoic acid over 400 mA cm^{-2}, Energy Environ. Sci. 13 (2020) 4990–4999, https://doi.org/10.1039/d0ee02607g.

[30] S. Xing, Z. Liu, Q. Xue, S. Yin, F. Li, W. Cai, S. Li, P. Chen, P. Jin, H. Yao, Y. Chen, Rh nanoroses for isopropanol oxidation reaction, Appl. Catal. B: Environ. 259 (2019), 118082, https://doi.org/10.1016/j.apcatb.2019.118082.

[31] B. You, X. Liu, X. Liu, Y. Sun, Efficient H2 evolution coupled with oxidative refining of alcohols via a hierarchically porous nickel bifunctional electrocatalyst, ACS Catal. 7 (2017) 4564–4570, https://doi.org/10.1021/acscatal.7b00876.

[32] Y. Ding, Q. Xue, Q.L. Hong, F.M. Li, Y.C. Jiang, S.N. Li, Y. Chen, Hydrogen and potassium acetate co-production from electrochemical reforming of ethanol at ultrathin cobalt sulfide nanosheets on nickel foam, ACS Appl. Mater. Interfaces 13 (2021) 4026–4033, https://doi.org/10.1021/acsami.0c20554.

[33] Y. Xu, M. Liu, S. Wang, K. Ren, M. Wang, Z. Wang, X. Li, L. Wang, H. Wang, Integrating electrocatalytic hydrogen generation with selective oxidation of glycerol to formate over bifunctional nitrogen-doped carbon coated nickel-molybdenum-nitrogen nanowire arrays, Appl. Catal. B: Environ. 298 (2021), 120493, https://doi.org/10.1016/j.apcatb.2021.120493.

[34] Y. Huang, X. Chong, C. Liu, Y. Liang, B. Zhang, Boosting hydrogen production by anodic oxidation of primary amines over a NiSe nanorod electrode, Angew. Chem. Int. Ed. Engl. 57 (2018) 13163–13166, https://doi.org/10.1002/anie.201807717.

[35] Y. Ding, B.-Q. Miao, S.-N. Li, Y.-C. Jiang, Y.-Y. Liu, H.-C. Yao, Y. Chen, Benzylamine oxidation boosted electrochemical water-splitting: Hydrogen and benzonitrile co-production at ultra-thin Ni2P nanomeshes grown on nickel foam, Appl. Catal. B: Environ. 268 (2020), 118393, https://doi.org/10.1016/j.apcatb.2019.118393.

[36] H.-Y. Sun, G.-R. Xu, F.-M. Li, Q.-L. Hong, P.-J. Jin, P. Chen, Y. Chen, Hydrogen generation from ammonia electrolysis on bifunctional platinum nanocubes electrocatalysts, J. Energy Chem. 47 (2020) 234–240, https://doi.org/10.1016/j.jechem.2020.01.035.

[37] L. Gao, Z. Liu, J. Ma, L. Zhong, Z. Song, J. Xu, S. Gan, D. Han, L. Niu, NiSe@NiOx core-shell nanowires as a non-precious electrocatalyst for upgrading 5-hydroxymethylfurfural into 2,5-furandicarboxylic acid, Appl. Catal. B: Environ. 261 (2020), 118235, https://doi.org/10.1016/j.apcatb.2019.118235.

[38] A. Tirsoaga, M. El Fergani, N. Nuns, P. Simon, P. Granger, V.I. Parvulescu, S. M. Coman, Multifunctional nanocomposites with non-precious metals and magnetic core for 5-HMF oxidation to FDCA, Appl. Catal. B: Environ. 278 (2020), 119309, https://doi.org/10.1016/j.apcatb.2020.119309.

[39] I.T. McCrum, M.T.M. Koper, The role of adsorbed hydroxide in hydrogen evolution reaction kinetics on modified platinum, Nat. Energy 5 (2020) 891–899, https://doi.org/10.1038/s41560-020-00710-8.
[40] Y. Cheng, H. Guo, P. Yuan, X. Li, L. Zheng, R. Song, Self-supported bifunctional electrocatalysts with Ni nanoparticles encapsulated in vertical N-doped carbon nanotube for efficient overall water splitting, Chem. Eng. J. 413 (2021), 127531, https://doi.org/10.1016/j.cej.2020.127531.
[41] C. Liang, P. Zou, A. Nairan, Y. Zhang, J. Liu, K. Liu, S. Hu, F. Kang, H.J. Fan, C. Yang, Exceptional performance of hierarchical Ni–Fe oxyhydroxide@NiFe alloy nanowire array electrocatalysts for large current density water splitting, Energy Environ. Sci. 13 (2020) 86–95, https://doi.org/10.1039/c9ee02388g.
[42] H. Xu, C. Shan, X. Wu, M. Sun, B. Huang, Y. Tang, C.-H. Yan, Fabrication of layered double hydroxide microcapsules mediated by cerium doping in metal–organic frameworks for boosting water splitting, Energy Environ. Sci. 13 (2020) 2949–2956, https://doi.org/10.1039/d0ee02113j.
[43] Z. Huang, S. Yuan, T. Zhang, B. Cai, B. Xu, X. Lu, L. Fan, F. Dai, D. Sun, Selective selenization of mixed-linker Ni-MOFs: NiSe2@NC core-shell nano-octahedrons with tunable interfacial electronic structure for hydrogen evolution reaction, Appl. Catal. B: Environ. 272 (2020), 118976, https://doi.org/10.1016/j.apcatb.2020.118976.
[44] T.V.M. Sreekanth, G.R. Dillip, P.C. Nagajyothi, K. Yoo, J. Kim, Integration of Marigold 3D flower-like Ni-MOF self-assembled on MWCNTs via microwave irradiation for high-performance electrocatalytic alcohol oxidation and oxygen evolution reactions, Appl. Catal. B: Environ. 285 (2021), 119793, https://doi.org/10.1016/j.apcatb.2020.119793.
[45] X. Deng, M. Li, Y. Fan, L. Wang, X.-Z. Fu, J.-L. Luo, Constructing multifunctional 'Nanoplatelet-on-Nanoarray' electrocatalyst with unprecedented activity towards novel selective organic oxidation reactions to boost hydrogen production, Appl. Catal. B: Environ. 278 (2020), 119339, https://doi.org/10.1016/j.apcatb.2020.119339.
[46] L. Bai, Y. Zhang, W. Tong, L. Sun, H. Huang, Q. An, N. Tian, P.K. Chu, Graphene for energy storage and conversion: synthesis and interdisciplinary applications, Electrochem. Energy R. 3 (2019) 395–430, https://doi.org/10.1007/s41918-019-00042-6.
[47] Y. Xu, M. Wang, K. Ren, T. Ren, M. Liu, Z. Wang, X. Li, L. Wang, H. Wang, Atomic defects in pothole-rich two-dimensional copper nanoplates triggering enhanced electrocatalytic selective nitrate-to-ammonia transformation, J. Mater. Chem. A 9 (2021) 16411–16417, https://doi.org/10.1039/d1ta04743d.
[48] H.F. Wang, L. Chen, H. Pang, S. Kaskel, Q. Xu, MOF-derived electrocatalysts for oxygen reduction, oxygen evolution and hydrogen evolution reactions, Chem. Soc. Rev. 49 (2020) 1414–1448, https://doi.org/10.1039/c9cs00906j.
[49] Y. Xu, X. Chai, T. Ren, S. Yu, H. Yu, Z. Wang, X. Li, L. Wang, H. Wang, Ir-Doped Ni-based metal-organic framework ultrathin nanosheets on Ni foam for enhanced urea electro-oxidation, Chem. Commun. 56 (2020) 2151–2154, https://doi.org/10.1039/c9cc09484a.
[50] Y. Xu, S. Yu, T. Ren, S. Liu, Z. Wang, X. Li, L. Wang, H. Wang, Hydrophilic/aerophobic hydrogen-evolving electrode: NiRu-based metal-organic framework nanosheets In situ grown on conductive substrates, ACS Appl. Mater. Interfaces 12 (2020) 34728–34735, https://doi.org/10.1021/acsami.0c03333.
[51] Y. Sun, Z. Xue, Q. Liu, Y. Jia, Y. Li, K. Liu, Y. Lin, M. Liu, G. Li, C.-Y. Su, Modulating electronic structure of metal-organic frameworks by introducing atomically dispersed Ru for efficient hydrogen evolution, Nat. Commun. 12 (2021) 1369, https://doi.org/10.1038/s41467-021-21595-5.
[52] X. Gao, Y. Yu, Q. Liang, Y. Pang, L. Miao, X. Liu, Z. Kou, J. He, S.J. Pennycook, S. Mu, J. Wang, Surface nitridation of nickel-cobalt alloy nanocactoids raises the performance of water oxidation and splitting, Appl. Catal. B: Environ. 270 (2020), 118889, https://doi.org/10.1016/j.apcatb.2020.118889.
[53] J. Chen, J. Liu, J.-Q. Xie, H. Ye, X.-Z. Fu, R. Sun, C.-P. Wong, Co-Fe-P nanotubes electrocatalysts derived from metal-organic frameworks for efficient hydrogen evolution reaction under wide pH range, Nano Energy 56 (2019) 225–233, https://doi.org/10.1016/j.nanoen.2018.11.051.
[54] H. Huang, S. Zhou, C. Yu, H. Huang, J. Zhao, L. Dai, J. Qiu, Rapid and energy-efficient microwave pyrolysis for high-yield production of highly-active bifunctional electrocatalysts for water splitting, Energy Environ. Sci. 13 (2020) 545–553, https://doi.org/10.1039/c9ee03273h.
[55] X. Liu, W. Li, X. Zhao, Y. Liu, C.W. Nan, L.Z. Fan, Two birds with one stone: metal–organic framework derived micro-/nanostructured Ni2P/Ni hybrids embedded in porous carbon for electrocatalysis and energy storage, Adv. Funct. Mater. 29 (2019), 1901510, https://doi.org/10.1002/adfm.201901510.
[56] X. Wen, J. Guan, Recent progress on MOF-derived electrocatalysts for hydrogen evolution reaction, Appl. Mater. Today 16 (2019) 146–168, https://doi.org/10.1016/j.apmt.2019.05.013.
[57] X. Wei, S. Wang, Z. Hua, L. Chen, J. Shi, Metal-organic framework nanosheet electrocatalysts for efficient H2 production from methanol solution: methanol-assisted water splitting or methanol reforming? ACS Appl. Mater. Interfaces 10 (2018) 25422–25428, https://doi.org/10.1021/acsami.8b06948.
[58] J. Hao, J. Liu, D. Wu, M. Chen, Y. Liang, Q. Wang, L. Wang, X.-Z. Fu, J.-L. Luo, In situ facile fabrication of Ni(OH)2 nanosheet arrays for electrocatalytic co-production of formate and hydrogen from methanol in alkaline solution, Appl. Catal. B: Environ. 281 (2021), 119510, https://doi.org/10.1016/j.apcatb.2020.119510.
[59] D.-J. Li, Q.-H. Li, Z.-G. Gu, J. Zhang, A surface-mounted MOF thin film with oriented nanosheet arrays for enhancing the oxygen evolution reaction, J. Mater. Chem. A 7 (2019) 18519–18528, https://doi.org/10.1039/c9ta04554f.
[60] Y. Li, X. Wei, L. Chen, J. Shi, M. He, Nickel-molybdenum nitride nanoplate electrocatalysts for concurrent electrolytic hydrogen and formate productions, Nat. Commun. 10 (2019) 5335, https://doi.org/10.1038/s41467-019-13375-z.
[61] S. Geiger, O. Kasian, M. Ledendecker, E. Pizzutilo, A.M. Mingers, W.T. Fu, O. Diaz-Morales, Z. Li, T. Oellers, L. Fruchter, A. Ludwig, K.J.J. Mayrhofer, M.T.M. Koper, S. Cherevko, The stability number as a metric for electrocatalyst stability benchmarking, Nat. Catal. 1 (2018) 508–515, https://doi.org/10.1038/s41929-018-0085-6.
[62] D. Muthuraj, A. Ghosh, A. Kumar, S. Mitra, Nitrogen and sulfur doped carbon cloth as current collector and polysulfide immobilizer for magnesium-sulfur batteries, ChemElectroChem 6 (2018) 684–689, https://doi.org/10.1002/celc.201801526.
[63] S.-C. Huang, C.-C. Cheng, Y.-H. Lai, C.-Y. Lin, Sustainable and selective formic acid production from photoelectrochemical methanol reforming at near-neutral pH using nanoporous nickel-iron oxyhydroxide-borate as the electrocatalyst, Chem. Eng. J. 395 (2020), 125176, https://doi.org/10.1016/j.cej.2020.125176.
[64] J. Jiang, F. Sun, S. Zhou, W. Hu, H. Zhang, J. Dong, Z. Jiang, J. Zhao, J. Li, W. Yan, M. Wang, Atomic-level insight into super-efficient electrocatalytic oxygen evolution on iron and vanadium co-doped nickel (oxy)hydroxide, Nat. Commun. 9 (2018) 2885, https://doi.org/10.1038/s41467-018-05341-y.
[65] J. Li, R. Wei, X. Wang, Y. Zuo, X. Han, J. Arbiol, J. Llorca, Y. Yang, A. Cabot, C. Cui, Selective methanol-to-formate electrocatalytic conversion on branched nickel carbide, Angew. Chem. Int. Ed. Engl. 59 (2020) 20826–20830, https://doi.org/10.1002/anie.202004301.
[66] J. Li, C. Xing, Y. Zhang, T. Zhang, M.C. Spadaro, Q. Wu, Y. Yi, S. He, J. Llorca, J. Arbiol, A. Cabot, C. Cui, Nickel iron diselenide for highly efficient and selective electrocatalytic conversion of methanol to formate, Small 17 (2021), 2006623, https://doi.org/10.1002/smll.202006623.
[67] B. Zhao, J. Liu, X. Wang, C. Xu, P. Sui, R. Feng, L. Wang, J. Zhang, J.-L. Luo, X.-Z. Fu, CO_2-emission-free electrocatalytic CH3OH selective upgrading with high productivity at large current densities for energy saved hydrogen co-generation, Nano Energy 80 (2021), 105530, https://doi.org/10.1016/j.nanoen.2020.105530.
[68] Q. Qian, Y. Li, Y. Liu, Y. Guo, Z. Li, Y. Zhu, G. Zhang, Hierarchical multi-component nanosheet array electrode with abundant NiCo/MoNi4 heterostructure interfaces enables superior bifunctionality towards hydrazine oxidation assisted energy-saving hydrogen generation, Chem. Eng. J. 414 (2021), 128818, https://doi.org/10.1016/j.cej.2021.128818.
[69] T. Ren, K. Ren, M. Wang, M. Liu, Z. Wang, H. Wang, X. Li, L. Wang, Y. Xu, Concave-convex surface oxide layers over copper nanowires boost electrochemical nitrate-to-ammonia conversion, Chem. Eng. J. 426 (2021), 130759, https://doi.org/10.1016/j.cej.2021.130759.
[70] K. Xiang, D. Wu, X. Deng, M. Li, S. Chen, P. Hao, X. Guo, J.L. Luo, X.Z. Fu, Boosting H2 generation coupled with selective oxidation of methanol into value-added chemical over cobalt hydroxide@hydroxysulfide nanosheets electrocatalysts, Adv. Funct. Mater. 30 (2020), 1909610, https://doi.org/10.1002/adfm.201909610.
[71] L. Tian, Z. Li, X. Xu, C. Zhang, Advances in noble metal (Ru, Rh, and Ir) doping for boosting water splitting electrocatalysis, J. Mater. Chem. A 9 (2021) 13459–13470, https://doi.org/10.1039/d1ta01108a.